

Full transient response of Taylor cones to a step change in electric field

Weiwei Deng · Alessandro Gomez

Received: 21 July 2011 / Accepted: 5 September 2011 / Published online: 28 September 2011
© Springer-Verlag 2011

Abstract We studied experimentally the complete transient response of Taylor cones subject to a step change in external electric field with the goal of finding optimal conditions to reduce the overall response time and achieve the highest possible switching bandwidth. The transient behavior of electrified menisci is of interest for many applications that would benefit from active control of on/off switching of the electrospray, such as femtoliter droplet-on-demand or novel fuel injectors in next generation internal combustion engines. We first investigated the transient behavior of ethanol, a typical solvent for droplet-on-demand. We then expanded the study to fuels such as JP-8 and E-30 biogas, a biofuel with 30% ethanol (vol.). The system response is a multi-stage process that can last from $\sim 100 \mu\text{s}$ to $\sim 100 \text{ms}$. Potential bottleneck stages include liquid accumulation, meniscus oscillation, and cone relaxation, depending on the experimental conditions. A typical full response time is $\sim 1 \text{ms}$, and the shortest transient process observed is $\sim 400 \mu\text{s}$. For a given liquid, nozzle outer diameter (OD) and applied voltage are the two most important parameters to influence the full response time. Onset or near-onset voltage for the establishment of the cone jet often leads to a large number of oscillation cycles and should be avoided. Changes in conductivity and viscosity by less than a factor of 10 have negligible effects

on the transient process. Using JP-8 or E-30 biogas, 90 μm OD nozzle with extractor, and flow rate of 0.4 mL/h, we can routinely achieve bandwidth of 1 kHz, corresponding to a full response time of 1 ms, after which quasi-monodispersed droplets of $\sim 10 \mu\text{m}$ are generated. Adaptation of an inviscid model of a charged oscillating droplet to the oscillating meniscus satisfactorily explains several key phenomena observed in our experiments, such as the full response time and the overshoot of the meniscus height.

1 Introduction

Electrospray (ES) is a liquid atomization method that has attracted growing interest, mainly because of the phenomenal size range of the particles that it can produce, from molecular dimensions to hundreds of microns (Gomez and Deng 2011). Among several possible ES operating modes, the most remarkable, widely used and extensively studied is the *cone-jet* mode (Cloupeau and Prunet-Foch 1990). In this mode, an intense electric field is applied to a nozzle and, through the combined effect of electric stress and interfacial tension, the liquid meniscus takes the shape of a cone which is termed Taylor cone (Taylor 1964). A fine jet issues from the apex of the Taylor cone and eventually breaks up into a spray of monodisperse droplets. The cone-jet ES produces monodisperse particles (Fernández de la Mora et al. 1990; Tang and Gomez 1994; Chen et al. 1995) with relative ease, which is a unique capability in the nanometric scale range. Recent progress in microfabricated multiplexed ES (MES) has overcome the critical drawback of low ES throughput (Deng et al. 2006, 2009). Multiplexed ES allows for the dispersion of large total flow rates through multiple, densely packed ES sources operating in parallel and uniformly, that is, delivering

W. Deng (✉)
Department of Mechanical, Materials, and Aerospace
Engineering, University of Central Florida, 4000 Central Florida
Blvd, Orlando, FL 32816, USA
e-mail: Weiwei.Deng@ucf.edu

A. Gomez (✉)
Department of Mechanical Engineering and Materials Science,
Yale University, 9 Hillhouse Ave., New Haven, CT 06520, USA
e-mail: Alessandro.Gomez@yale.edu

droplets of the same size from each nozzle. Thus, MES expands the applications of ES beyond electrospray ionization mass spectroscopy (Fenn et al. 1989). A wide range of MES applications in combustion (Deng et al. 2006), material synthesis (Almería et al. 2010, 2011), electric propulsion (Lenguito et al. 2010), and spray cooling (Deng and Gomez 2011) have recently been reported.

The vast majority of the ES literature is devoted to the steady cone-jet mode since continuous operation is needed in many cases. However, emerging applications may require quick and even repetitive transition from off (no atomization) to on (stable cone-jet mode). One example is the electrohydrodynamically pulsed jet (Choi et al. 2008; Kang et al. 2011) for droplet-on-demand, which extends the droplets size from nano/pico-liters of traditional ink-jet printing to femtoliter droplets. Another application is the controlled deposition through digital electrospray (Deng et al. 2010), in which any individual ES can be turned on or off in a 61-nozzle array. Transient electrospray may also find applications in fuel injection in homogeneous charge compression ignition (HCCI) engine, in which the small diameter, monodispersity, and Coulombic repulsion of fuel droplets are expected to improve engine performance (Anderson et al. 2008).

The pulsing mode of Taylor cones at fixed voltages is relatively well understood (Juraschek and Röllgen 1998; Marginean et al. 2004, 2006; Chen et al. 2006; Gubarenko et al. 2008; Chiarot et al. 2008, 2009; Choi et al. 2008). In (Marginean et al. 2004), the authors used time-lapse images to reveal a four-phase process of the pulsing Taylor cone: liquid accumulation, cone formation, ejection of liquid jet, and relaxation. In a subsequent study (Marginean et al. 2006), those authors characterized the charge of the pulsating Taylor cone by relating the measured pulsing frequency to the frequency spectrum for the capillary waves on the surface of a charged droplet (Rayleigh 1882). Scaling laws relating pulsing frequency to the applied electric field were obtained by deriving a charge accumulation time in a single pulsing cycle (Chen et al. 2006) or by balancing the normal electric stress to the surface tension (Choi et al. 2008). For anchored liquid meniscus subject to AC electric field, Wang et al. (2006) reported remarkable polyhedral shapes formation of a resonant drop excited at different modes of the Rayleigh–Lamb dispersion.

A systematic investigation of the complete transient process from an anchored hemispherical meniscus fed at a constant flow rate to a steady Taylor cone is still missing. This article focuses on such a response to a step change in external electric field. We aim to identify geometric and physical parameters controlling the entire transient response and implement the fastest practical response in scalable microfabricated, out-of-plane circular silicon nozzles, with potential application in fuel atomization. We

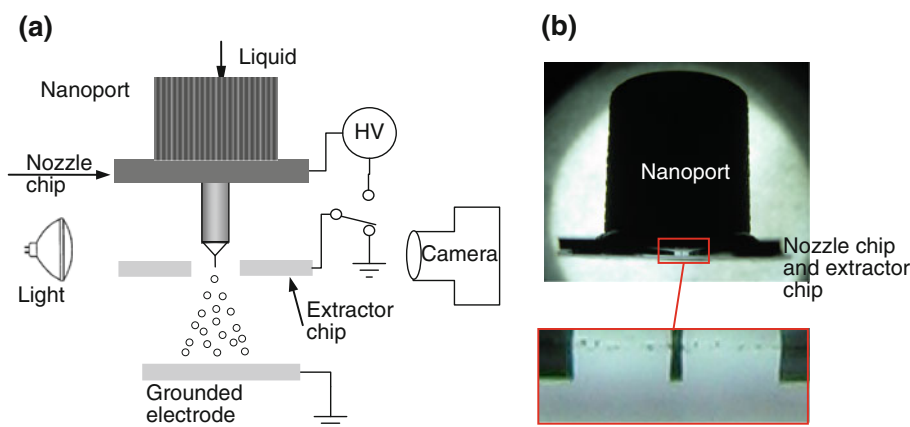
first investigate the process using ethanol as a benchmark liquid, because it has good electrospray properties and is a typical solvent in many ES applications. Then, we expand the study to other liquids of interest in engine applications such as JP-8 and biogasoline. We also explore a reasonably broad parameter space and scaling laws that can guide us toward design and operating conditions leading to shorter response time in a broader range of transient ES applications, beyond the original focus on fuel mixtures of potential interest in automotive applications. We finally propose a meniscus damping model to satisfactorily explain several key phenomena observed in the reported experiments.

2 Experimental setup

Figure 1 shows the experimental setup. We adopted the nozzle–extractor configuration that is typical of the MES (Deng et al. 2006, 2009; Bocanegra et al. 2006). Both nozzle chip and extractor were microfabricated using a tailored deep reactive ion etch (DRIE) in the US Army Research Laboratory (ARL), with typical microfabrication flow documented elsewhere (Deng et al. 2009). The tested nozzle OD are 60, 90, and 180 μm . We achieved precise alignment of the extractor and the nozzle by using optical fibers as alignment aid. The fibers would rest in opposing trenches etched in the nozzle chip and the extractor chip. The tight diameter tolerance of the optical fiber dimension enables both alignment and gap control by lithographically tailoring the width of the alignment trenches, and the circular fiber cross section provides self-centering alignment between the two stacked components. The alignment accuracy is estimated to be better than 1 μm . In addition, the optical fiber serves as electrical insulator to maintain a ~ 1 kV nozzle–extractor voltage difference. The nozzle/extractor assembly (Fig. 1b) was glued to a nanoport (Upchurch) which allows for liquid input with a small dead volume. The on/off switch is connected to the extractor. The voltage step-change response of the switch is ~ 5 μs , which is a few orders of magnitude faster than the transient response of a Taylor cone to a step change in the external electric field. At start-up, we first ran the syringe pump without switching on the electric field, with the high-speed camera on. Once we observed the first pinch-off of a drop from the meniscus suspended at the tip of the nozzle, we stopped the syringe pump. This moment was set as the starting point of the experiment. We then switched on the e-field and the syringe pump simultaneously.

A relatively wide channel around the nozzle was etched on the nozzle chip to improve the optical illumination, which is critical for shooting high-speed videos with a shutter time as short as 1 μs . The channel also reduces the

Fig. 1 Experimental setups for transient response of Taylor cones: **a** test arrangement for high speed imaging; **b** nozzle chip assembly, with zoomed-in view of the single nozzle. The distance between the nozzle tip and the extractor is typically 100 μm, and the distance between the extractor and the grounded electrode is 10 mm



disturbance due to image reflection between the two parallel chip surfaces.

A high-speed camera (Phantom v7.3) coupled through a bellow to a microscope objective lens is aimed at the tip of the nozzle. The magnification of the imaging system is adjusted by varying the distance between the lens and the camera sensor. Typical magnifications used are 12× for the 180-μm OD device, and 25× for smaller nozzles. The camera framing rate is 100,000 fps at the resolution of 128 × 128, or 250,000 fps at 64 × 64 for smaller nozzles. In both cases, the shutter time is 1 μs.

We tested seven liquids with different conductivities: pure ethanol, ethanol doped with either 30 or 100 ppm by weight of an ionic liquid (IL) (1-ethyl-3-methylimidazolium ethylsulfate), ethylene glycol, JP-8 doped with 0.1% Statis450 (Dupont), iso-octane with 30% ethanol, and iso-octane with 15% ethanol. Flow rates range from 0.03 to 0.6 mL/h per nozzle, depending on the liquid tested. Key physical properties are reported in Table 1.

The liquid was pumped continuously into the reservoir by a syringe pump (Harvard apparatus) with different syringe sizes to ensure that the plunger would be displaced at a reproducible and accurate speed. To verify the establishment of the cone-jet mode, droplet size and two velocity components were measured by an optical

fiber phase Doppler particle analyzer (PDPA, TSI) from the scattering of a frequency-modulated argon ion laser beam (Coherent). At steady cone-jet mode or after the completion of the transient process, the PDPA measurement shows good quasi-monodispersity of the droplet diameter, with a typical relative standard deviation of 10%.

3 General behavior of transient Taylor cones

3.1 Phenomenological overview

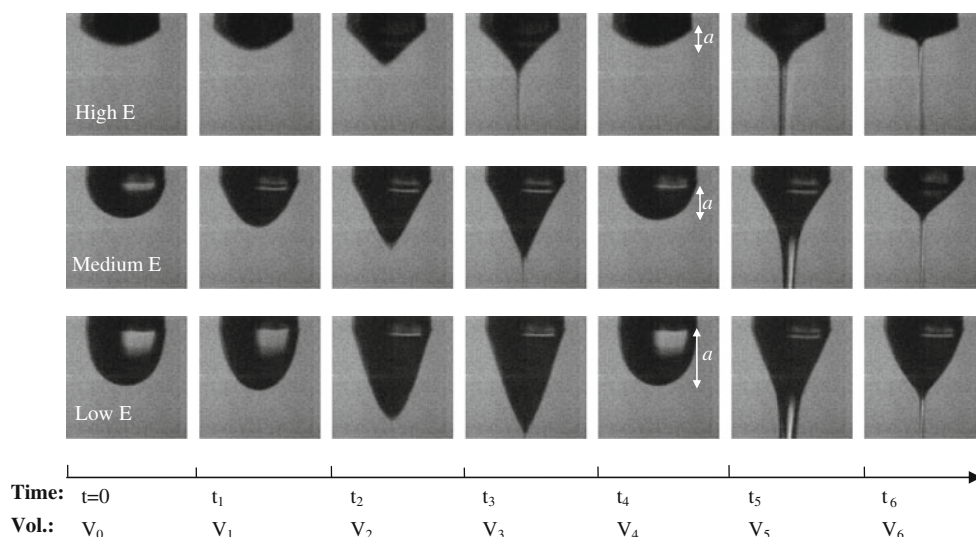
The full transient response of the liquid meniscus to a step change of electric field consists of multiple sequential processes as illustrated in Fig. 2 for high, intermediate, and low electric fields (*E*), respectively.

Before *t* = 0, no electric field is applied since both the nozzle and the extractor are at identical electric potentials. The meniscus is suspended at the nozzle tip forming a spherical cap. The height of the suspended meniscus is shorter for higher applied voltages, which is due to a change in the liquid contact angle at the rim of the nozzle tip. A change in height, in turn, results in a different meniscus volume *V*₀.

Table 1 Physical properties of tested liquids

Name	Ethl	IL-30	IL-100	EG	JP8-S	E-30	E-15
Composition	Ethanol	Ethanol + 30 ppm IL	Ethanol + 100 ppm IL	Ethylene glycol	JP8 + 0.1% Statis450	Iso-octane + 30% ethl	Iso-octane + 15% ethl
Conductivity <i>K</i> (10 ⁻⁵ S/m)	1.3	7.5	240	2.4	0.26	0.47	0.02
Mass density <i>ρ</i> (g/cm ³)	0.789	0.789	0.789	1.11	0.8	0.7	0.7
Viscosity (cP)	1.2	1.2	1.2	16.1	3.5	0.88	0.88
Surface tension (mN/m)	22.4	22.4	22.4	47.7	28	21	21

Fig. 2 Typical transient response of the liquid meniscus subject to a step change of electric field at different field intensities. Liquid is pure ethanol; flow rate is 0.4 mL/h; nozzle OD is 180 μm ; operating voltages are 1,200 V (high E), 1,000 V (medium E) and 850 V (low E); camera speed is 100,000 fps



At $t = 0$, the electric field is applied to the liquid meniscus by connecting the extractor to the ground. At t_1 , shortly after the electric field is applied, the meniscus deforms from a spherical cap to a prolate hemispheroid with the meniscus tip still rounded. The volume V_1 is essentially identical to V_0 , because of the short t_1 . From t_1 to t_2 , the meniscus gradually develops into a cone with a sharper and sharper tip as the liquid is fed into the meniscus continuously, until the volume reaches a critical value V_2 . At t_3 , which is typically 10 μs after t_2 , a jet erupts from the fully developed cone. Depending on the electric field, the jet may detach from the cone and the cone may relax back to a hemispherical shape at t_4 . This eruption–relaxation cycle may repeat itself several times (Marginean et al. 2004), until the jet no longer detaches at t_5 . Thereafter, the cone gradually shrinks to V_6 at t_6 and later it is indistinguishable from that of the steady cone-jet mode.

A short response time can be achieved only through a careful selection of the operating conditions to minimize each of these five stages, as explained below.

3.2 RC response time, t_{RC}

The nozzle–extractor connected to the high voltage is equivalent to a RC circuit with a characteristic response time $t_{RC} = RC$. The resistance R is due mainly to the contact between the silicon extractor and the power supply, with a typical value of 1 $\text{M}\Omega$ for a good contact. The capacitance is due to the two parallel conductive planes (the nozzle chip and the extractor chip) close to each other, and can be expressed as $C = \epsilon A/s$, where ϵ is the permittivity of the dielectric media (air in this work), A is the chip area, and s is the gap between the nozzle chip to the extractor. For a $12.7 \times 12.7 \text{ mm}^2$ chip with 300- μm gap, a typical capacitance is 4 pF. Therefore, the RC response

time in our experiment is $\sim 4 \mu\text{s}$, which is much shorter than the entire transient process ($\sim 1 \text{ ms}$) and hence negligible.

In the present work, the RC response time is not a limiting factor. However, in general, for silicon devices care should be taken to ensure that resistance and capacitance are small. In fact, a thin SiO_2 layer naturally develops on the Si surface in air and provides some electric insulation. On the extractor, a good contact is still possible by scratching the chip surface and exposing the silicon. However, it is virtually impossible to do so for the inner surface of the nozzle. Therefore, if one tries to switch the high voltage on/off on the nozzle chip instead of the extractor, the resistance will be increased dramatically because the nozzle is not in direct contact with the high voltage (HV) source due to the thin SiO_2 layer, and the HV must go through the fine liquid column in the nozzle, generating a high resistance of more than 1 $\text{G}\Omega$. As a result, the RC time becomes $> 4 \text{ ms}$, which is longer than a typical transient time of a Taylor cone in this work and unacceptably large.

3.3 Liquid accumulation time, t_a

t_a is defined as the time required for the syringe pump to supply enough liquid to change the volume of the meniscus from V_1 to V_2 , that is $t_a = t_2 - t_1 = (V_2 - V_1)/Q$, when liquid evaporation is neglected (here, Q is the liquid flow rate supplied by the pump). When either a very high or a very low electric field is applied, V_1 and V_2 are significantly different and $(V_2 - V_1) \sim V_2 \sim \text{OD}^3/4$. We have listed several typical t_a s in Table 2.

The data in Table 2 suggest that the accumulation time may span a large range, from 0.3 to 54 ms, and is primarily determined by the OD. Consequently, the liquid accumulation stage can be a significant component of the entire

Table 2 Liquid accumulation time for different combinations of nozzle ODs and flow rates

OD (μm)	180	180	90	90	60	60
Q (mL/h)	0.6	0.1	0.6	0.1	0.6	0.1
<i>t_a</i> (ms)	9	54	1	6	0.3	1.5

transient process. Table 2 is consistent with our experimental results, which revealed typically 4 ms accumulating time for 180-μm OD nozzles, and 1 ms for 90-μm OD nozzles under either very high or very low electric fields. For example, for kHz response frequency, we need to operate the electrospray with a nozzle OD ≤ 90 μm and with a relatively high flow rate of ~0.6 mL/h.

At extremely high electric fields, the Taylor cone anchors to the edge of the inner diameter (ID). Typically ID ≈ OD/2, which reduces the accumulation volume by one order of magnitude and dramatically reduces the accumulating time. But ID anchoring is not highly repeatable and hence is not recommended. On the other hand, it is beneficial to adopt microfabrication recipes yielding tapered nozzles, which may reduce the OD by 50% and achieve a one order of magnitude reduction in accumulation time.

The accumulation time can also be greatly reduced by applying an appropriate electric field. At an intermediate electric field, it is possible to achieve (V₂ - V₁) ~ 0.1V₂, which makes this accumulation negligible as compared to other times. We routinely achieved 0.3 ms accumulation time for 180-μm OD nozzles, and 0.1 ms for 90-μm OD nozzles with suitably chosen electric fields.

3.4 Eruption time, *t_e*

The eruption time *t_e* = *t₃* - *t₂* is a very quick process taking only about ~10 μs for all experimental conditions, including different nozzle ODs, flow rates, and electric field intensities. It appears to be the shortest stage in the entire transient process.

3.5 Single-cycle oscillation time *t_{osc}*

Before the liquid meniscus settles to the steady state cone-jet mode, it may oscillate several times, switching back and forth between a cone-jet morphology and a hemisphere. Each single cycle lasts *t_{osc}* = *t₄* - *t₃*. A closely related phenomenon is the classic problem of the angular frequency of oscillation for a droplet carrying the electrical charge *q* (Rayleigh 1882):

$$\omega^2 = \frac{l(l-1)}{\rho a^3} \left[(l+2)\gamma - \frac{q^2}{16\pi^2 \epsilon_0 a^3} \right], \tag{1}$$

where *l* is the oscillation mode and its value is an integer greater than 1, *a* is the radius of the droplet, ρ is the liquid

mass density, γ is the liquid–air interfacial tension, and ϵ_0 is the air permittivity. Mathematically, *l* is the order of the Legendre polynomials *P_l*(cosθ). The dominant mode of oscillation is *l* = 2, and at this mode the Rayleigh limit $q^2 < q_R^2 = 64\pi^2 \epsilon_0 \gamma a^3$ can be recovered. A droplet charged at a fraction β of the Rayleigh limit ($q^2 = \beta q_R^2$) was predicted to oscillate at

$$\omega_c = \sqrt{8(1-\beta)\gamma/\rho a^3}. \tag{2}$$

In the present work, we choose the meniscus height *a* instead of the nozzle OD as the characteristic length for two reasons. First, the meniscus mass, which obviously affects the oscillating frequency, is proportional to *a* for fixed nozzle OD. Second, *a* depends on the intensity of applied electric field, with a higher electric field leading to a smaller *a*. Thus, when using *a* as the characteristic length, both the electrode separation and applied voltage are factored in and do not need to be addressed separately.

Strictly speaking, Eq. (1) is applicable to free droplets with small oscillating amplitude. Practically, Eq. (1) has been applied with satisfactory accuracy in characterizing a pulsating Taylor cone, which is an anchored meniscus that deforms between a hemispherical and conical shape (Margein et al. 2006). We compared Eq. (2) to the experiment to see whether it could appropriately describe the oscillation of the electrified liquid meniscus. Note that now the characteristic length *a* may vary by a factor of up to two, depending on the applied electric field. Figure 3 shows single-cycle oscillation time *t_{osc}* recorded for different ODs, flow rates, and electric fields. The data span more than one order of magnitude in *t_{osc}*. The experimental data approximately collapse on a trend line $t_{osc} \propto a^{3/2}$, capturing the essential relationship between the oscillation frequency and the size of the meniscus. Moreover, the fitted straight line yields β = 0.59, corresponding to the oscillation of a meniscus charged at 59% of the Rayleigh limit.

Since the oscillation time of a single cycle scales with *a^{3/2}*, this time can change by as much as a factor of 3 for the same nozzle under different electric fields. From this point of view, a more intense electric field is preferred to reduce *t_{osc}*. However, other factors, such as the accumulation time, should also be considered in selecting the electric field.

3.6 Overall oscillation time *t_{ove}*

The overall oscillation time is determined by *t_{ove}* = (*N* + 1)·*t_{osc}*, where *N* is the number of oscillation cycles the meniscus has to experience before the jet is permanently attached to the cone.

Experimentally, we can identify two distinct electric field conditions affecting *N*. The first one appears near the

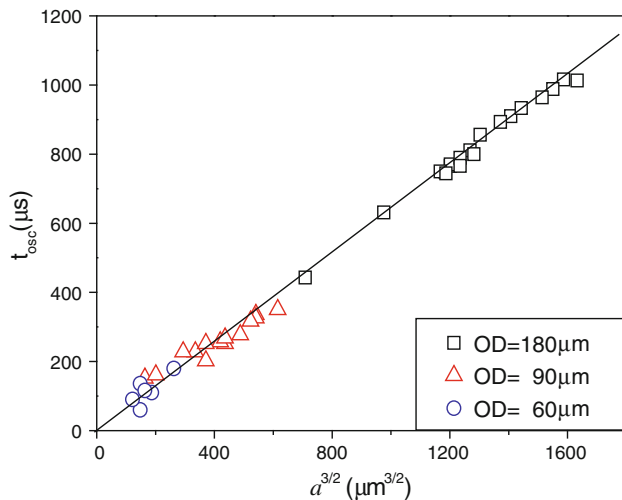


Fig. 3 Oscillation time versus the 3/2 power of the liquid meniscus height

onset voltage, where N is usually as large as $\sim 10^3$, and t_{ove} may be as long as ~ 100 ms, which appears unnecessarily long. The other extreme is at intermediate or high electric field, under which N is only one or even zero for most cases. On the other hand, Fig. 3 suggests that the t_{osc} is larger than $100 \mu\text{s}$, which is likely to be the dominant stage in the transient process. Therefore, unity or even zero N is favorable for quick response and fast switching frequencies. This provides another incentive to operate the electro-spray far away from the onset voltage.

3.7 Relaxation time, t_r

The last stage of the transient process is the relaxation one, during which the cone-jet gradually shrinks to the steady state morphology, usually with a smaller final cone volume V_6 . Similar to the oscillation stage, the liquid meniscus may vibrate and the diameter of the attached jet may fluctuate with large amplitude. The vibration is most obvious near the onset voltage, under which the jet diameter can fluctuate by a factor of three. The duration of the vibration $t_r = t_6 - t_5$ is difficult to quantify, and it can last over 100 ms, similar to the oscillation stage near onset voltage.

At higher electric fields, the number of vibrations is very small, typically less than three, and the relaxation time is controlled by the viscous time $\tau_\mu = \rho a^2 / \mu$, where μ is the liquid viscosity. Moreover, the cone-jet can be identified as “usable” even before it is fully relaxed to steady state, if the goal is to generate supermicron droplets. The argument is as follows: the volume change from V_5 to V_6 is due to the shrinkage of the cone height, which is typically $OD/3$. Therefore, $\Delta V = (V_5 - V_6) \sim OD^3/8$. The viscous damping time is $\tau_\mu \sim t_r \sim \rho a^2 / \mu \sim \rho OD^2 / \mu$, and the average flow rate difference during this period is

$\Delta Q = \Delta V / \tau_\mu \sim \mu OD / 8\rho$. This average flow rate is equivalent to 0.05 mL/h for a 90- μm OD nozzles, and only counts for 10% of the typical flow rate of 0.5 mL/h. In terms of droplet size, the effect will be even more modest. Therefore, in practical applications, t_5 may mark the end of the transient process at intermediate and high electric fields.

3.8 An ideal scenario

The complete transient process consists of multiple stages, several of which can last a relatively long (>10 ms) time. However, these stages could be optimized to expedite the overall transient process. Particularly, the accumulation time t_a , the overall oscillation time t_{ove} , as well as the relaxation time t_r , can be reduced without altering essential electro-spray properties. One sample case is for the 90- μm OD device operated at intermediate electric field and relatively high flow rate (0.6 mL/h). The times for the different stages are listed in Table 3. The entire transient process only takes 392 μs that is equivalent to 2.5 kHz.

4 Parametric study on nozzle diameter and liquid physical properties

4.1 Optimal nozzle outer diameter for fast transient process

The nozzle OD is the most critical geometric parameter for the transient process because multiple processes strongly depend on OD. A small OD is preferable to reduce t_a and t_{osc} . However, practical considerations impose a lower limit on the OD. First, the nozzle must keep some mechanical strength. The weakest part of the nozzle is at the base, where the maximum stress is experienced when a load is applied to the nozzle. Furthermore, microfabrication recipes using DRIE approach often result in undercutting of the Si nozzles, yielding nozzles that are thinner at the base, which further exacerbates the mechanical strength challenge. The stress is proportional to the inverse of the moment of inertia, or OD^{-4} . Therefore, the stress at the nozzle base increases dramatically as the OD is reduced. Our experience with the current microfabrication process is that even simple ultrasonication cleaning of 30- μm OD nozzles presents a high risk of nozzle breaking, while 60- μm OD devices are relatively robust and safe. Second, among the devices tested, a significant reduction in transient time was achieved when the OD was decreased from 180 to 90 μm , with a much more modest reduction when the OD was further reduced to 60 μm . Therefore, we consider a 90- μm OD nozzle a balanced choice for quick transient response time, good mechanical strength and ease

Table 3 An ideal case of fast transient response with a 90- μm OD device

Stage	RC response	Accumulation	Eruption	Single oscillation	Overall oscillation	Relaxation	Total
Notation	t_{RC}	t_a	t_e	t_{osc}	t_{ove}	t_r	t_{total}
Time (μs)	4	100	8	150	150	140	392

of visualization. Of course, if the fabrication recipe were changed yielding tapered devices at the tip, further reductions would ensue at no cost in mechanical robustness of the device.

4.2 Effect of liquid electric conductivity and viscosity

We tested seven liquids with different electrical conductivities (K) spanning four orders of magnitude, from 10^{-7} to 10^{-3} S/m, as shown in Table 1. In this section, we focus on pure ethanol and ethanol doped with either 30 or 100 ppm of IL. They are intended to represent a hypothetical case, in which the conductivity of the solvent is altered in potential droplet-on-demand applications. Except

for K , other relevant liquid physical properties, such as surface tension and viscosity, are essentially unchanged by the addition of IL. Figure 4 shows a comparison of the oscillation time (one cycle) of ethanol and ethanol +100 ppm IL (IL-100 in short). We notice that IL-100 oscillates $\sim 30\%$ faster than pure ethanol and, despite the drastic change in conductivity by $>100\times$, the change in t_{osc} is still modest. Using Eq. (2), we can infer that the meniscus of the IL-100 has lower average charge level than that of pure ethanol. We also noticed that for IL-100, the meniscus experiences a large number of oscillations and the entire response time is >10 ms. The intermediate case of ethanol with 30 ppm of IL (Fig. 5b), resulting in a factor of 6 increase in conductivity, is compared to that of pure ethanol (Fig. 5a) in terms of full setting time versus applied voltage. The transient response is very similar to that of pure ethanol: in both cases, the response time is dramatically longer at the onset voltage, and a typical response time is 500–2,000 μs .

The different behavior caused by the change in conductivity may be interpreted in terms of relative magnitude of charge relaxation time $\tau_r = \epsilon/K$ and hydrodynamic time $\tau_h \sim a/u \sim \mu \cdot a/\gamma$, where u is a characteristic velocity obtained by balancing viscous and surface tension forces; that is, $\mu \cdot u/a$ and γ/a , respectively. For pure ethanol, $\tau_h \sim 5 \mu\text{s}$ and $\tau_r = 16 \mu\text{s}$. For IL30, τ_h is still $5 \mu\text{s}$, but $\tau_r = 2.7 \mu\text{s}$. In both cases, the charge relaxation time and the hydrodynamic time are comparable. However, for IL100, τ_r is only ~ 100 ns, which is much shorter than τ_h . This simple scaling may help rationalizing different transient behaviors as K is significantly modified.

We also used ethylene glycol to investigate the effect of viscosity. Qualitatively, a change by a factor of 16 in

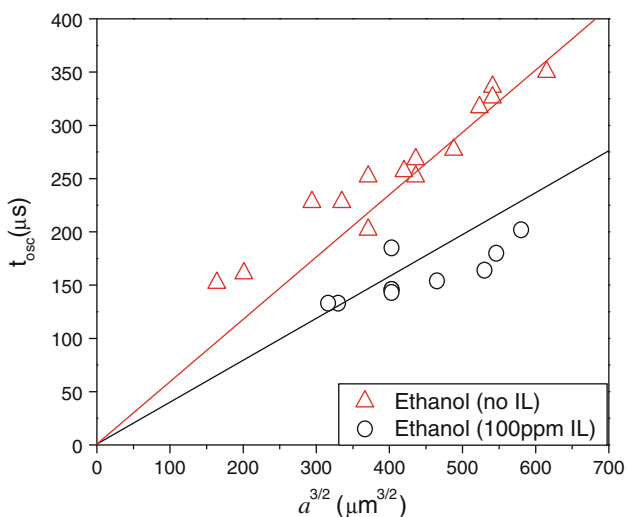
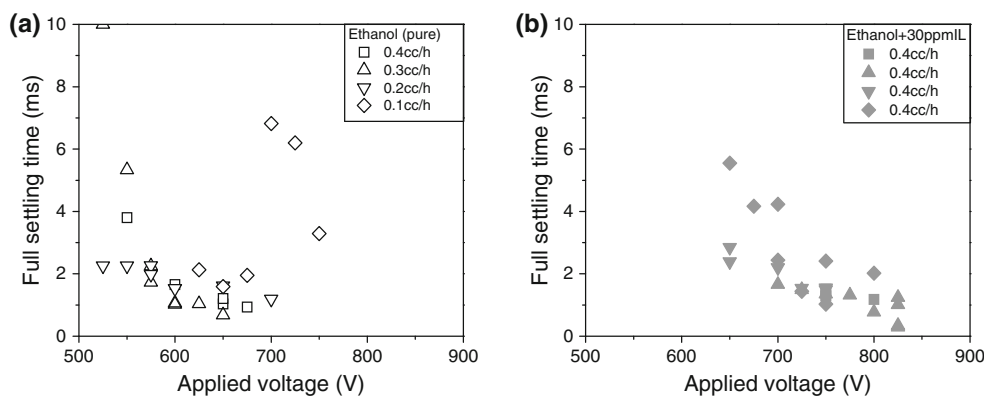


Fig. 4 Single cycle oscillation time of ethanol ($K = 1.3 \times 10^{-5}$ S/m) and ethanol doped with IL-100 ($K = 2.4 \times 10^{-3}$ S/m)

Fig. 5 Full response time at various voltage and flow rates for **a** pure ethanol ($K = 1.3 \times 10^{-5}$ S/m) and **b** IL-30 ($K = 7.5 \times 10^{-5}$ S/m)



viscosity does not cause a significant change in transient process time. For example, the average full response time of 11 tests of ethylene glycol Taylor cones on 90- μm OD nozzle is 4.7 ms, which is in the range of pure ethanol and IL30 shown in Fig. 5.

5 Transient response of JP-8 and bio-fuel surrogates

To make JP-8 electro-sprayable, we typically add a small amount of Statis450 as a conductivity enhancer. With 0.1% concentration, $K = 2.6 \times 10^{-6}$ S/m, which is $\sim 1/5$ that of ethanol. Figure 6 shows a Taylor cone of ethanol and of the doped JP-8, both operating at 0.2 mL/h. The ethanol cone appears to be approximately equipotential, while the cone of JP-8 has a curved profile, which suggests that it is not equipotential as a result of the low conductivity. The voltage required for JP-8 to establish a cone-jet is $\sim 40\%$ higher than for ethanol.

Despite the large difference in conductivity and shape of the cone, the overall transient behavior of doped JP-8 is very similar to that of ethanol, both qualitatively and quantitatively. First, the full response time of the JP8 meniscus is of the same order as that of ethanol, i.e., 1,000 μs as compared to 2,000 μs (Fig. 7a). Second, the oscillation time also shows a linear relationship with respect to $a^{3/2}$ (Fig. 7b). Furthermore, the fitted line in

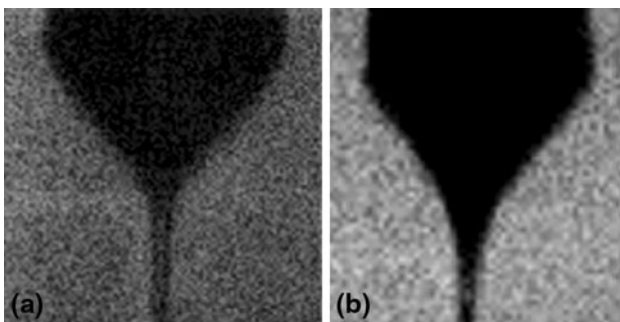


Fig. 6 Steady Taylor cone of ethanol (a) and JP-8 (b). Nozzle OD is 90 μm

Fig. 7 Transient behavior of JP-8: **a** Full response time at various voltage and flow rates; **b** single cycle oscillation time

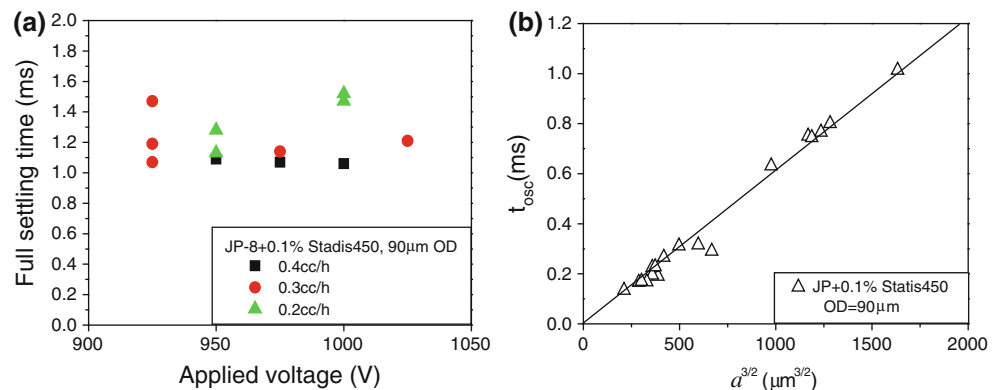


Fig. 7b gives $\beta = 0.63$, corresponding to the oscillation of a meniscus charged at 63% of the Rayleigh limit.

We also tested two types of biofuel surrogates: E-30 and E-15. E-30 has a conductivity similar to that of doped JP-8 and is suitable for electro-spray, whereas the conductivity of E-15 is so low that it takes a very long time (~ 10 ms) to form the Taylor cone. In terms of response time versus applied voltage, E-30 (Fig. 8a) behaves similarly to ethanol, has a wide range of operating voltage, from 625 to 900 V, and exhibits a response time clearly dependent on applied voltage: the higher the voltage, the shorter is the full response time.

The oscillation time still scales linearly with $a^{3/2}$ (Fig. 8b), and the slope is smaller than that of ethanol or JP-8, which is attributable to the lower density of iso-octane.

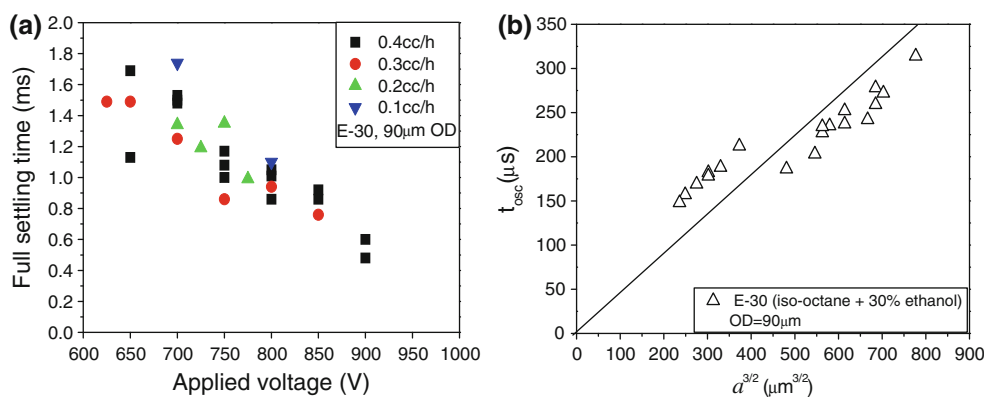
6 A meniscus damping model

We have shown that the multiple oscillation stage appears to be the limiting factor to reduce the overall transient response time. In this section, we focus on quantitatively describing the damping of the oscillation process by analogy with a simple model of an oscillating droplet. The goal is to identify key parameters that will lead to short overall response time.

6.1 Small-amplitude droplet oscillation

The oscillation of a charged droplet has been studied extensively dating back to the pioneering work of Lord Rayleigh (1882), as, for example in (Saville 1974; Marginean et al. 2004; Zeng and Korsmeyer 2004; Chen et al. 2006; Wang et al. 2006; Choi et al. 2008; and Paine 2008). Here, we assume that the suspended meniscus behaves similarly to free oscillating droplets, and we choose the meniscus height a as the characteristic length. Following (Saville 1974), we write the velocity potential functions Ψ inside the droplet with small amplitude surface deformation in spherical coordinates as

Fig. 8 Transient behavior of E-30: **a** full response time at various voltage and flow rates; **b** single cycle oscillation time



$$\Psi(r, \theta, \varphi, t) = \psi(r, \theta, \varphi)e^{-\omega t}, \tag{3}$$

where $\psi(r, \theta, \varphi)$ satisfies Laplace’s equation. Therefore, $\psi(r, \theta, \varphi)$ can be expressed by Legendre polynomials $P_l(\cos\theta)$ or spherical harmonics $Y_l^m(\theta, \varphi)$, with $l = 0, 1, 2, \dots$. Here, ω is the complex oscillation frequency

$$\omega = \zeta\omega_n + i\omega_c, \tag{4}$$

where $\omega_n = (8\gamma/\rho a^3)^{1/2}$ is the undamped natural frequency (with $\beta = 0$ in Eq. 2), ζ is a dimensionless number defined as damping ratio, and $\omega_c = \omega_n(1 - \zeta^2)^{1/2}$ is the damped natural frequency. The real part of Eq. (4) measures how quickly the system is damped, while the imaginary part of Eq. (4) describes the oscillation property.

Figure 9 illustrates the oscillation stages of the Taylor cone and their correspondence to a typical step response of a second-order system. The transient Taylor cone shows a behavior similar to a second-order system, with meniscus height $a(t)$ characteristically representing the process status. For an underdamped system with $\zeta < 1$, the meniscus will oscillate for several cycles before it

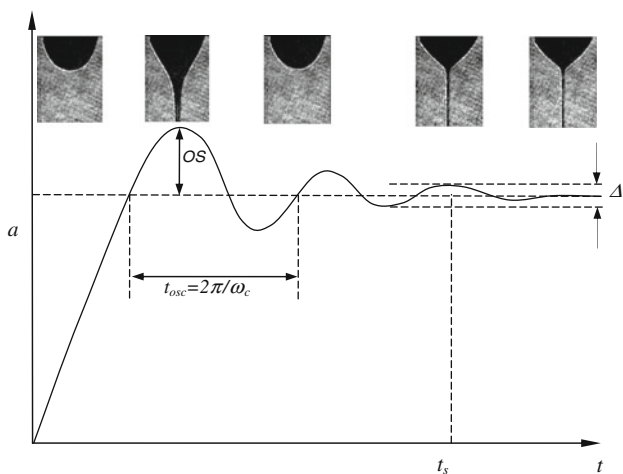


Fig. 9 Comparison of the deformation of the anchored meniscus with a typical step response of a second-order system. Here, a represents the height of the meniscus and t is the time elapsed

stops. For an overdamped system, with $\zeta > 1$, the meniscus will stop the oscillation slowly. For a critically damped system $\zeta = 1$, the meniscus reaches its equilibrium position in the shortest possible time. Furthermore, if we compare the imaginary part of Eq. (4) with Eq. (2), we obtain

$$\zeta = \beta^{1/2}. \tag{5}$$

Equation (5) suggests that the damping ratio is $\beta^{1/2}$, i.e., the surface charge density normalized by the Rayleigh limit. Experimental results suggest that the less conductive liquid has a higher β values. We recall three distinctive damping behaviors that correspond to high, medium, and low conductivity:

1. High K : with IL-100, the system appears to be extremely underdamped because the response time is very long.
2. Medium K : with pure ethanol, the system is modestly damped with a relatively fast response time.
3. Low K : with E-15, the meniscus appears to be overdamped since the Taylor cone takes a very long time to develop.

These observations are consistent with the theoretical analysis in (Saville 1974), in which the electrical shearing stresses are found to affect the nature of the damping substantially. A similar concept is also described in (Shiryaeva et al. 2007), where the authors found that taking into account the effect of electric charge relaxation leads to an aperiodic instability.

This strong dependence on the electric conductivity suggests that the charge relaxation time $\tau_r = \epsilon/K$ plays an important role in the damping ratio. A long charge relaxation time makes the charge redistribute more slowly, which causes the electric stress to act on the meniscus more slowly, making damping more obvious. On the other hand, a very short charge relaxation time will lead to immediate charge redistribution upon a change in the external electric field, and the electric stress can be applied to the meniscus

without substantial delays. This is equivalent to a very modest damping effect.

Equation (5) also suggests that the damping ratio solely depends on the fraction of the Rayleigh limit, and the liquid viscosity does not appear to provide any damping effect. This seemingly counterintuitive conclusion can be explained by general scaling considerations: the viscous time $\tau_\mu \sim \rho a^2/\mu$ is much longer than the single cycle oscillation time $\tau_{\text{osc}} \sim (\rho a^3/\gamma)^{1/2}$. For example, with $a = 100 \mu\text{m}$ for ethanol, $\tau_\mu \sim 10 \text{ ms}$ and τ_{osc} is only $\sim 0.2 \text{ ms}$. As a result, during each single cycle the fluid appears to be inviscid. Viscosity may intervene in the last relaxation stage, when the cone-jet gradually shrinks to the steady-state shape, but, as discussed in Sect. 3.7, that stage is of modest relevance to the size of the generated droplets.

6.2 Overshoot and settling time

The normalized charge level (β) can be inferred from the oscillation time measurement of an electrified meniscus, such as Figs. 4, 7b and 8b. Then, the damping ratio ζ can be determined. For example, Fig. 4 suggests that with 90- μm OD, the damping ratios for pure ethanol is $\zeta = 0.77$, and for IL-100 $\zeta = 0.09$. The first damping ratio is of unity order, which suggests that a significant damping effect takes place, consistently with experimental observations for pure ethanol. The second damping ratio is close to zero, which suggests that the system is very weakly damped, as also confirmed by the transient behavior of IL-100.

As for a second-order system, we can derive a dimensionless overshoot parameter, OS, and the settling time t_s for oscillating electrified meniscus. Here, we only consider an underdamped system.

The overshoot is the amount that the waveform (meniscus height in our case) overshoots the steady-state value (the height of final Taylor cone). It is important for the transient ES because of the potential for jet detachment. If the OS is too large, during the relaxation phase jet pinching and breakup may happen, which may significantly deteriorate size monodispersity and prolong the full response time. Presently, we do not have knowledge of the critical OS value for jet detachment. Nonetheless, we can still compute OS for two typical cases (pure ethanol and IL-100) with the following equation (Marlin 1995):

$$\text{OS} = \exp(-\pi\zeta/\sqrt{1-\zeta^2}). \quad (6)$$

Equation (6) suggests that dimensionless overshoot is a function only of the damping ratio. For pure ethanol, $\text{OS} = 0.02$, whereas for IL-100, $\text{OS} = 0.75$, corresponding to a large overshoot. In terms of experimental observations, we did see routinely no jet detachment for pure ethanol, while multiple jet detachments for IL-100.

The settling time t_s is the time required for damped oscillations to reach and stay within Δ of the steady-state value. Δ may be regarded as a tolerance, for which a reasonable choice may be 2%. In our experiments, t_s is approximately $t_6 - t_1$. The formula to evaluate the settling time is (Marlin 1995):

$$t_s = -\ln \Delta/\zeta\omega_n = -(\ln \Delta/2\pi) \cdot \tau_{\text{osc}}/\zeta \sim \tau_{\text{osc}}/\zeta. \quad (7)$$

Therefore, for pure ethanol ($\zeta = 0.77$) the settling time is comparable to the meniscus oscillation time. For IL-100 ($\zeta = 0.09$), the settling time is about one order of magnitude larger than the meniscus oscillation time.

We conclude by underscoring that this model does not apply at very low voltages. The oscillations at low voltage are in the vicinity of the pulsing regime, corresponding to an infinite number of oscillations. As a result, the proposed settling model is only applicable at voltages well above the onset voltage of the cone-jet mode (Tang and Gomez 1994).

7 Conclusions

We examined the complete transient response of Taylor cones subject to a step change in external electric field. Fluids tested include ethanol, ethylene glycol, JP-8 with 0.1% Statis450 and biofuel with 30% ethanol (vol.). Although the emphasis was on a potential combustion application, a sufficiently broad parameter range was explored to generalize some of the observations. All liquids work reasonably well and behave similarly in terms of full response time and oscillation time. The system response is a multi-stage process that can last from $\sim 100 \mu\text{s}$ to $\sim 100 \text{ ms}$. Potential bottleneck stages include liquid accumulation, meniscus oscillation, and cone relaxation, depending on the experimental conditions. A typical full response time is $\sim 1 \text{ ms}$, and the shortest transient process observed is $\sim 400 \mu\text{s}$.

For a given liquid, nozzle OD and applied voltage are the two most important parameters to influence the full response time. An OD of 90 μm is a balanced choice for fast response and sufficient mechanical strength. An outer diameter smaller than 60 μm does not shorten the response time significantly. Onset or near-onset voltage often leads to a large number of oscillation cycles and should be avoided. Changes in conductivity and viscosity by less than a factor of 10 have negligible effects on the transient process.

The adaptation of an inviscid model of charged oscillating droplet to the oscillating meniscus satisfactorily explains several key phenomena observed in our experiments, such as the full response time and overshoot of the meniscus height.

Using JP-8 or E-30 biogas, 90- μm OD nozzle with extractor, 0.4 mL/h/nozzle, and sub-1 kV voltage, we can routinely achieve full response times of 1 ms, after which quasi-monodispersed droplets (with a typical relative standard deviation of 10%) of $\sim 10\ \mu\text{m}$ are generated. As an example of a potential application, the settling time of 1 ms only accounts for $<10\%$ of the temporal pulse width of fuel injection in a typical HCCI engine, suggesting that it is feasible to use the multiplexed electrospray technology in such engines for a benchmark study on the role of atomization on engine performance.

Acknowledgments The support of the US Army under Cooperative Agreement No. W911NF-05-2-0015 (Dr. C. Mike Waits, Contract Monitor) is gratefully acknowledged. We wish to thank Dr. C. Mike Waits and B. Hanrahan for the microfabrication work that was carried out at the Army Research Laboratory (MD, USA).

References

- Almería B, Deng W, Fahmy T, Gomez A (2010) Controlling the morphology of electrospray-generated PLGA microparticle for drug delivery. *J Colloid Interface Sci* 343:125–133
- Almería B, Fahmy T, Gomez A (2011) A multiplexed electrospray process for single-step synthesis of stabilized polymer particles for drug delivery. *J Control Release* 154:203–210
- Anderson EK, Koch JA, Kyritsis DC (2008) Phenomenology of electrostatically charged droplet combustion in normal gravity. *Combust Flame* 154:624–629
- Bocanegra R, Galán D, Márquez M, Loscertales IG, Barrero A (2006) Multiple electrospays emitted from an array of holes. *J Aerosol Sci* 36:1387–1399
- Chen D, Pui DYH, Kaufman SL (1995) Electrospaying of conducting liquids for monodisperse aerosol generation in the 4 nm to 1.8 m diameter range. *J Aerosol Sci* 26:963–977
- Chen C-H, Saville DA, Aksay IA (2006) Scaling laws for pulsed electrohydrodynamic drop formation. *Appl Phys Lett* 89 no. 12: 124103
- Chiarot PR, Gubarenko SI, Ben Mrad R, Sullivan P (2008) Application of an equilibrium model for an electrified fluid interface: electrospray using a PDMS microfluidic device. *J Microelectromech Syst* 17:1362–1375
- Chiarot PR, Gubarenko SI, Ben Mrad R, Sullivan P (2009) On the pulsed and transitional behavior of an electrified fluid interface. *J Fluid Eng* 131:091202
- Choi HK, Park J-U, Park OO, Ferreira PM, Georgiadis JG, Rogers JA (2008) Scaling laws for jet pulsations associated with high-resolution electrohydrodynamic printing. *Appl Phys Lett* 92:123109
- Cloupeau M, Prunet-Foch B (1990) Electrostatic spraying of liquids: main functioning modes. *J Electrostat* 25(2):165–184
- Deng W, Gomez A (2011) Electrospray cooling for microelectronics. *Int J Heat Mass transf* 54:2270–2275
- Deng W, Klemic JF, Li X, Reed M, Gomez A (2006) Increase of electrospray throughput using multiplexed microfabricated sources for the scalable generation of monodisperse droplets. *J Aerosol Sci* 37:696–714
- Deng W, Waits CM, Morgan B, Gomez A (2009) Compact multiplexing of monodisperse electrospays. *J Aerosol Sci* 40:907–918
- Deng W, Waits CM, Gomez A (2010) Digital electrospray for controlled deposition. *Rev Sci Instr* 81:35114
- Fenn JB, Mann M, Meng CK, Wong SF, Whitehouse CM (1989) Electrospray ionization for mass spectrometry of large biomolecules. *Science* 246(4926):64–71
- Fernández de la Mora J, Navascues J, Fernández F, Rosell Llompart J (1990) Generation of submicron monodisperse aerosols by electrospays. *J Aerosol Sci* 21(S1):s673–s676
- Gomez A, Deng W (2011) Chapter 20 fundamentals of Con-jet electrospray. In: Baron PA, Kulkarni P, Willeke K (eds) *The aerosol measurement: principles, techniques and applications*, 3rd ed. Wiley, New York
- Gubarenko SI, Chiarot PR, Ben Mrad R, Sullivan P (2008) Plane model of fluid interface rupture in an electric field. *Phys Fluids* 20:043601
- Juraschek R, Röllgen FW (1998) Pulsation phenomena during electrospray ionization. *Int J Mass Spectrom* 177:1
- Kang DK, Lee MW, Kim HY, James SC, Yoon SS (2011) Electrohydrodynamic pulsed-inkjet characteristics of various inks containing aluminum particles. *J Aerosol Sci* 42(10):621–630
- Lenguito G, Fernandez de la Mora J, Gomez A (2010) Multiplexed electrospray for space propulsion applications, 46th AIAA Joint Propulsion Conference, AIAA-2010-6521
- Marginean L, Parvin L, Heffernan, Vertes A (2004) Flexing the electrified meniscus: the birth of a jet in electrospays. *Anal Chem* 76:4202
- Marginean I, Nemes P, Parvin L, Vertes A (2006) How much charge is there on a pulsating Taylor cone? *Appl Phys Lett* 89:064104
- Marlin TE (1995) *Process control: designing processes and control systems for dynamic performance*, McGraw-Hill, pp 242–245
- Paine MD (2008) Transient electrospray behaviour following high voltage switching. *Microfluid Nanofluid* 6:775–783
- Rayleigh L (1882) On the equilibrium of liquid conducting masses charged with electricity. *Philos Mag* 14:184–186
- Saville DA (1974) Electrohydrodynamic oscillation and stability of a charged drop. *Phys Fluids* 17:54–60
- Shiryaeva SO, Grigor'ev AI, Kryuchkov OS (2007) On the oscillations of a charged drop of a finite-conductivity viscous liquid. *Tech Phys* 52(6):690–698
- Tang K, Gomez A (1994) On the structure of an electrostatic spray of monodisperse droplets. *Phys Fluids A* 6(7):2317–2332
- Taylor G (1964) Disintegration of water drops in an electric field. *Proc Royal Soc London* 280(1382):383–397
- Wang P, Maheshwari S, Chang H-C (2006) Polyhedra formation and transient cone ejection of a resonant microdrop forced by an ac electric field. *Phys Rev Lett* 96:254502
- Zeng J, Korsmeyer T (2004) Principles of droplet electrohydrodynamics for lab-on-a-chip. *Lab Chip* 4:265